



ARTICLE

Development and application of a cultivation platform for mammalian suspension cell lines with single-cell resolution

Julian Schmitz¹ | Sarah Täuber¹ | Christoph Westerwalbesloh² |
Eric von Lieres² | Thomas Noll³ | Alexander Grünberger¹

¹Multiscale Bioengineering, Faculty of Technology, Bielefeld University, Bielefeld, Germany

²Institute of Bio- and Geosciences, IBG-1: Biotechnology, Forschungszentrum Jülich GmbH, Jülich, Germany

³Cell Culture Technology, Faculty of Technology, Bielefeld University, Bielefeld, Germany

Correspondence

Alexander Grünberger, Multiscale Bioengineering, Faculty of Technology, Bielefeld University, Universitätsstraße 25, 33615 Bielefeld, Germany.
Email: alexander.gruenberger@uni-bielefeld.de

Abstract

In bioproduction processes, cellular heterogeneity can cause unpredictable process outcomes or even provoke process failure. Still, cellular heterogeneity is not examined systematically in bioprocess research and development. One reason for this shortcoming is the applied average bulk analyses, which are not able to detect cell-to-cell differences. In this study, we present a microfluidic tool for mammalian single-cell cultivation (MaSC) of suspension cells. The design of our platform allows cultivation in highly controllable environments. As a model system, Chinese hamster ovary cells (CHO-K1) were cultivated over 150 h. Growth behavior was analyzed on a single-cell level and resulted in growth rates between 0.85 and 1.16 day⁻¹. At the same time, heterogeneous growth and division behavior, for example, unequal division time, as well as rare cellular events like polynucleation or reversed mitosis were observed, which would have remained undetected in a standard population analysis based on average measurements. Therefore, MaSC will open the door for systematic single-cell analysis of mammalian suspension cells. Possible fields of application represent basic research topics like cell-to-cell heterogeneity, clonal stability, pharmaceutical drug screening, and stem cell research, as well as bioprocess related topics such as media development and novel scale-down approaches.

KEYWORDS

mammalian cell lines, microfluidics, single-cell cultivation, suspension cell culture

1 | INTRODUCTION

Traditionally, analytical investigations in bioprocess research and development have been realized by bulk measurements. Consequently, every discovery and technical advancement is based on averaged population values determined over millions of cellular events (Templer & Ces, 2008; Wang & Bodovitz, 2010). As a result, individual behavior of nonconform-acting cells in a genetically

identical population remains masked behind average values, which, therefore, do not depict every cell's nature (Lecault et al., 2012; Lindström & Andersson-Svahn, 2010; Yin & Marshall, 2012). In the last few years, these cellular heterogeneities have received increasing awareness in consideration of being the origin of manifold inconsistencies in bioprocess related affairs such as viability and productivity (Delvigne & Goffin, 2014). Moreover, in matters of biopharmaceutical production, heterogeneous behavior concerning

This is an open access article under the terms of the Creative Commons Attribution-NonCommercial License, which permits use, distribution and reproduction in any medium, provided the original work is properly cited and is not used for commercial purposes.

© 2020 The Authors. *Biotechnology and Bioengineering* published by Wiley Periodicals LLC

overall growth or product yield can have a severe impact on the process's robustness and reproducibility. Particularly when utilizing Chinese hamster ovary (CHO) cell lines, known genetic instability caused by the high rate of genetic changes can increase heterogeneous behavior additionally (Frye et al., 2016; Wurm, 2013). Of particular interest are properties like the loss of productivity (Le et al., 2012), single-cell growth behavior, and the occurrence of dormant cells during the bioprocess (Grünberger et al., 2015), as well as apoptotic and necrotic processes inside the bioreactor (Grilo & Mantalaris, 2019). Certainly, conventional process analytical technology can detect the outcome of these phenomena but has no opportunity for analyzing and understanding them, due to its lack of single-cell resolution and defined environmental conditions.

As a consequence of the rising interest in the behavior of individual cells during bioproduction applications, the number of single-cell analysis tools has increased over the last years (Schmitz et al., 2019). First approaches based on flow cytometry allow insights into single-cell behavior and population heterogeneity. However, a dynamic investigation of single cells is not feasible. Therefore, especially approaches utilizing polydimethylsiloxane (PDMS)-based microfluidic devices became popular over the last years because of the steadily evolving microfabrication and ongoing progress in the field of microfluidics (Halldorsson et al., 2015). Their potential to trap cells in diverse featured microfluidic structures in combination with live cell imaging results in a high spatial and temporal resolution of single-cell behavior (Grünberger et al., 2014; Rowat et al., 2009). Depending on the system's design, microfluidic approaches provide high throughput analysis with hundreds of replicates on one microfluidic device. In carefully designed setups, a high level of environmental control can be achieved and even dynamic changes in cultivation conditions, reagent concentration, or nutrient supply can be realized (Dettinger et al., 2018; Marques & Szita, 2017; Täuber et al., 2020).

Microfluidic single-cell analysis and cultivation have successfully been applied to examine bioprocess relevant questions of industrially relevant microbial host systems such as the influence of heterogeneity on cellular growth and production, the influence of specific media components, or bacterial coculture approaches (Binder et al., 2016; Burmeister et al., 2018; Unthan et al., 2014). Lately, microfluidic single-cell applications have likewise made their entry in the field of cell culture (Mehling & Tay, 2014). Examples of applications are transfection studies (Raimes et al., 2017) and cell line development (Bjork et al., 2015), cell interaction studies (Li et al., 2016), drug screening (Du et al., 2016), and stem cell research (Luni et al., 2016) where single-cell analysis expanded the previous state of knowledge. In general, microfluidic cultivation devices can be differentiated by their way of capturing and retaining single cells into traps, wells, or chambers (Figure 1). These setups have different system specifications that enable different applications. Microfluidic traps (Figure 1a) have been used, for example, in viability assays and morphology studies, focusing on single-cell behavior and not on microcolony growth (Di Carlo et al., 2006; Wheeler et al., 2003). The cells are located inside the medium stream, which allows a convective supply of nutrients

during the experiment but also holds the risk of shear stress. As cells are actively retained inside the trap, the cultivation of adherent as well as cells growing in suspension is realizable. In comparison to traps, the supply of nutrients in cultivation wells (Figure 1b) is diffusive and convective as cells are located inside the wells and are perfused across. Therefore, the cultivation of suspension cells is not feasible without washing them out frequently. Depending on well diameter, microcolony growth can be observed, which makes wells especially applicable for cell spreading, proliferation, differentiation, and cell interaction studies (Karakas et al., 2017; Lin et al., 2015). Cultivation chambers combine the advantages of traps and wells for the cultivation of cells (Figure 1c). Flow velocities inside the chambers are very low, meaning a large part of the nutrient supply takes place by diffusion and the cells are not exposed to significant shear stress. Although cultivation of adherent as well as suspension cells is conceivable, so far only adherently growing cells have been cultivated in chambers. Due to their characteristics which make long-term growth feasible, chambers have been applied in growth studies and drug screening (Gao et al., 2013; Kolnik et al., 2012).

Until now, most microfluidic single-cell applications for mammalian cell lines are limited to analytical questions in basic and applied research (Gao et al., 2013; Postiglione et al., 2016; Woodruff & Maerkl, 2016) but do not systematically address single-cell growth, media development, and process engineering in terms of bioprocess research and development (Schmitz et al., 2019). In contrast to the already existing microfluidic systems for the analysis of microbial hosts, systems for the analysis of mammalian cells do not offer the opportunity to systematically examine growth characteristics on a single-cell level for appropriate cultivation times. This is due to their focus on single-cell analysis applications, which consequently do not address important technical characteristics for the cultivation of single cells such as spatially defined cell trapping, continuous defined medium supply, and spatiotemporal resolution for live-cell imaging over the whole cultivation time. As a proof-of-concept, the first studies investigating long-term single-cell growth of adherent CHO and HeLa cell lines have been reported and showed comparable growth between microfluidic and lab-scale cultivation (Kolnik et al., 2012). Nevertheless, these systems were not applied for systematic growth studies of mammalian cell lines with full spatiotemporal resolution in the context of dynamic single-cell studies. An even larger drawback is the exclusive application of adherent growing cells in single-cell growth-related studies. As most bioproduction processes rely on in suspension growing cells (Wurm, 2004), results from single-cell cultivation of adherent growing cells are of limited relevance for this application. Consequently, single-cell cultivation of mammalian cells is not only hampered by the unavailability of appropriate setups but also by nonexistent studies of suspension cell lines in microfluidic applications.

In this study, we present a PDMS-glass-based microfluidic setup for long-term single-cell cultivation of CHO cells growing in suspension. This setup allows simultaneous analysis of growth characteristics and cellular heterogeneity under highly controlled environmental conditions. Using soft lithography, microfluidic chips

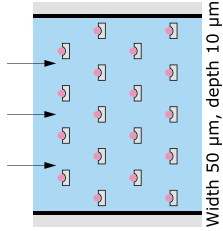
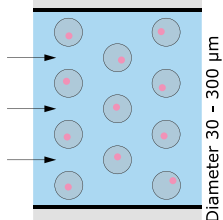
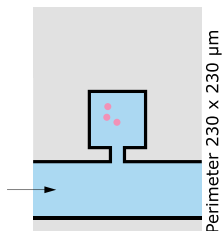
(a)				
Trap		Nutrient supply:	Convective	
		Culture properties:	Adherent & suspension	
		Application:	Viability assays, morphology studies	
		Cell type:	Lymphocytes, HeLa	
		Reference:	Wheeler et al. (2003), Di Carlo et al. (2006), etc.	
(b)				
Well		Nutrient supply:	Diffusive & convective	
		Culture properties:	Adherent	
		Application:	Cell spreading, proliferation, differentiation, interaction studies	
		Cell type:	Human carcinoma cells, HEK 293T	
		Reference:	Lin et al. (2015), Karakas et al. (2017), etc.	
(c)				
Chamber		Nutrient supply:	Diffusive	
		Culture properties:	Adherent	
		Application:	Growth studies, drug screening	
		Cell type:	Lymphocytes, CHO-K1, HeLa	
		Reference:	Kolnik et al. (2012), Gao et al. (2013), etc.	

FIGURE 1 Examples of microfluidic cultivation devices in the field of mammalian cell culture categorized into the underlying cell retention principle. Traps, wells, and chambers differ in the way cells are retained and supplied with nutrients, offer appropriate cultivation surfaces for either adherent or suspension cell lines, and support different applications. For every device examples of utilized cell types as well as representative studies are listed [Color figure can be viewed at wileyonlinelibrary.com]

were fabricated, which offer the possibility to capture and track single mammalian cells in isolated cultivation chambers. Adjacent perfused supply channels enable constant delivery of nutrients and removal of metabolic by-products, due to diffusive processes without exposing the cells to shear stress. Sufficient mass transfer was verified by computational fluid dynamics (CFD) simulations. The growth of CHO-K1 cells was investigated and evaluated on the single-cell level. The results show reproducible growth behavior, making mammalian single-cell cultivation (MaSC) an attractive single-cell cultivation device.

2 | MATERIAL AND METHODS

2.1 | Microfluidic device fabrication

Using two-layer photolithographic techniques described previously (Grünberger et al., 2013), a silicon wafer was produced as a mold for

PDMS chip fabrication. PDMS base and curing agent (SYLGARD 184 Silicone Elastomer; Dow Corning Corporation) were mixed in a ratio of 10:1, poured onto the silicon wafer, degassed by means of a desiccator, and cured for 2 h at 80°C. Afterward, the chips were cut, inlets and outlets were punched with a biopsy punch (Reusable Biopsy Punch, 0.75 mm; WPI), and particles were removed from PDMS chip and glass substrate (76 × 26 × 1 mm microscope slides; VWR International GmbH) via isopropanol washing and drying with pressurized air. To covalently link chip and glass, surfaces were activated by oxygen plasma (Femto Plasma Cleaner; Diener Electronics) and bonded to each other. Subsequently, the microfluidic device was incubated at 80°C for 1 min to enhance bonding.

2.2 | Computational fluid dynamics

Detailed CFD simulations were performed to model flow profiles within cultivation chambers and supply channels as well as to analyze

nutrient supply inside the microfluidic device. The computational model used in this study has been described in detail previously (Westerwalbesloh et al., 2015, 2017). The model geometry contains only one chamber and parts of the adjacent supply channels because the conditions within each chamber are assumed to be independent of its position on the microfluidic device. All CFD simulations were performed using COMSOL Multiphysics Version 5.4 (COMSOL AB). The flow field was determined by solving the steady-state Navier–Stokes equations for creeping (Stokes) flow of an isothermal, incompressible, and Newtonian liquid with the properties of water (density 993.22 kg/m³, viscosity 6.96 × 10⁻⁴ Pa s (interpolated for 37°C [Comesaña et al., 2003]). The no-slip condition was used at the PDMS and glass walls. Laminar inflow with a rate of 8.33 × 10⁻¹² m³/s was specified at each of the supply channel inlets, while the outlet condition was a reference pressure of 0 Pa. The glucose concentration field was calculated by solving the general steady-state diffusion–advection equation with a diffusion coefficient of 8.5 × 10⁻¹⁰ m²/s. Adsorption at the glass and PDMS walls was neglected. Due to the concentration of glucose being below 45 mol/m³ it could be assumed that the flow field is not influenced by the glucose concentration, and therefore flow and mass transfer were solved sequentially. In the model, the chamber is populated with cells (171 cells in a filled chamber on a typical microscope image). Every cell is assumed to take up glucose with a rate of 3800 nmol per 10⁶ cells and day (Nolan & Lee, 2011), which leads to a volumetric uptake rate of 2.4 × 10⁻² mol s⁻¹ m⁻³, distributing the cellular uptake homogeneously over the growth chamber. The geometry of the cells themselves is not explicitly included as shown before (Westerwalbesloh et al., 2017). The glucose concentration provided in the growth medium is assumed to be high enough to yield a constant (maximal) uptake rate in the model, independent of the exact local glucose concentration. The computational geometry was discretized using 106,176 rectangular elements. A finer mesh with 847,000 elements yielded the same results, indicating mesh independence of the solution (data not shown). Quadratic functions were used to calculate velocity profiles and concentrations and linear functions for the pressure.

2.3 | Cell culture and medium

Cultivation of CHO-K1 cells was performed in a commercially available cell culture medium (TCX6D; Xell), supplemented with 8 mM glutamine. Cultivation conditions for preculture were 37°C, 5% CO₂, 80% humidity, and 180 rpm in TubeSpin® Bioreactor 50 (TPP®) with a cultivation volume of 15 ml. CHO-K1 cells were subcultured every third and fourth day and viable cell density was adjusted to 1.5 × 10⁵ cells/ml. For microfluidic single-cell cultivation, fresh medium was mixed with conditioned medium in a ratio of 1:1. For the generation of conditioned medium, cells were cultivated according to the above protocol. The required volume of cell suspension was harvested from the same preculture that was prepared for starting the cultivation at the day of inoculation. In a first step the

cell suspension was centrifuged at 1500 rpm for 5 min. Finally, the resulting supernatant was additionally sterilely filtrated using a 0.2-µm cut-off filter (Filtropur S 0.2; Sarstedt AG & Co. KG).

2.4 | Microfluidic single-cell cultivation

Single-cell cultivation in microfluidic devices was performed on an automated inverted microscope (Nikon Eclipse Ti2; Nikon Instruments), enabling high-throughput time-lapse microscopy. Cultivation temperature was kept constant at 37°C by using a microscope incubator system (Cage incubator, OKO Touch; Okolab S.R.L.). An additional CO₂ incubation chamber (H201-K-FRAME GS35-M; Okolab S.R.L.) enabled a constant CO₂ atmosphere of 5% (95% compressed air). Monitoring growth and morphology was achieved by live-cell imaging: time-lapse images of relevant positions were taken every 20 min (NIS Elements AR 5.20.01 Software; Nikon Instruments) applying 40× objective with phase-contrast microscopy.

Cells were seeded into cultivation chambers by manually flushing the microfluidic chip with cell suspension until loading of the chambers was sufficient. Medium supply was realized by low-pressure syringe pumps (neMESYS; CETONI) and single-use syringes (Injekt® 10 ml; B. Braun Melsungen AG) connected to the chip via PTFE tubing. During cultivation, the medium was constantly perfused through the cultivation device with a flow rate of 2 µl/min.

2.5 | Image evaluation and growth analysis

Cell number was manually counted on time-lapse images every 10 h to evaluate growth behavior. The colony growth rate μ was estimated graphically by determining the slope of the linear regression from the resulting semi-logarithmic plot using OriginPro (OriginPro 2020 9.7.0.188; OriginLab Corporation). Under the assumption of exponential colony growth, Equation (1) was applied to convert μ to doubling times t_D

$$t_D = \frac{\ln(2)}{\mu}. \quad (1)$$

As the exponential growth of mammalian cell lines can be described by a geometric sequence, the respective mean values for t_D and μ were determined using the geometric mean (Phoenix, 1997). In comparison to the arithmetic mean, which is especially suitable for linear sequences, the geometric mean is less prone to the influence of outliers in a broad distribution of values. For quantification of single-cell doubling time distribution, single cells were tracked manually and the time span between two cell divisions was determined. The single-cell area was analyzed using ImageJ 1.52p (Schindelin et al., 2012). For determination of area growth, cellular contours on scaled microscope pictures were manually retraced. The cellular area was subsequently determined and plotted against cultivation duration. Analog to colony growth rates, these charts were used to determine area related single-cell growth rates. The calculation of possible correlations was performed according to Pearson.

3 | RESULTS AND DISCUSSION

3.1 | Device design and working principle

Derived from a previously introduced microbial system, the microfluidic device presented in this study was optimized for single-cell cultivation of mammalian cell lines in high throughput, with high spatiotemporal resolution, and at highly controlled environmental conditions. One microfluidic device consists of four independent cultivation arrays with one inlet and one outlet each for environmental interfacing (Figure 2a). Each array is composed of four parallel running supply channels with a width of $200\ \mu\text{m}$ (Figure 2b). Between two supply channels, 30 cultivation chambers with dimensions of $200 \times 200\ \mu\text{m}$ are arranged in line, summing up to 60 chambers in total per array. $50 \times 50\ \mu\text{m}$ entrances link the cultivation area with the supply unit of the array. Growth chambers and entrances are approximately $8\ \mu\text{m}$ high, while supply channels are designed with a height of $16\ \mu\text{m}$. The difference in height of the structures is intended to restrict flow from the channel into the chambers and facilitate cell retention inside the chamber. Likewise, the narrow chamber entrances improve withholding seeded cells.

As a result of the limited height, cellular growth inside the chamber is restricted to a monolayer. Resulting from its dimensions, the array's total volume sums up to approximately $2.3 \times 10^8\ \mu\text{m}^3$, equaling 230 nL. Due to the chip's fabrication using soft-lithography, silicon wafers with varying channel and chamber heights can easily be fabricated to adapt chip dimensions to specific scientific question and cell lines.

To capture single cells inside the cultivation chambers, cell suspension is flushed through the supply channels and cells randomly enter the chambers. As cell seeding is not actively controllable, loading efficiency meaning the percentage of seeded and empty chambers is directly connected to cell density of the inoculum. Here, concentrations around 30×10^5 cells/ml proved to be a reasonable compromise between loading efficiency and cell number per loaded chamber. If cell density is lower, only a few chambers are loaded with cells. If cell density is too high, the starting cell number exceeds one to five cells per chamber promoting nonisogenic microcolonies.

Once enough cultivation chambers are loaded with cells, constant perfusion of the array is initiated through the chip's inlet by syringe pumps (Figure 2c). With a steady flow of $2\ \mu\text{l}/\text{min}$, cells are constantly provided with fresh nutrients while metabolic

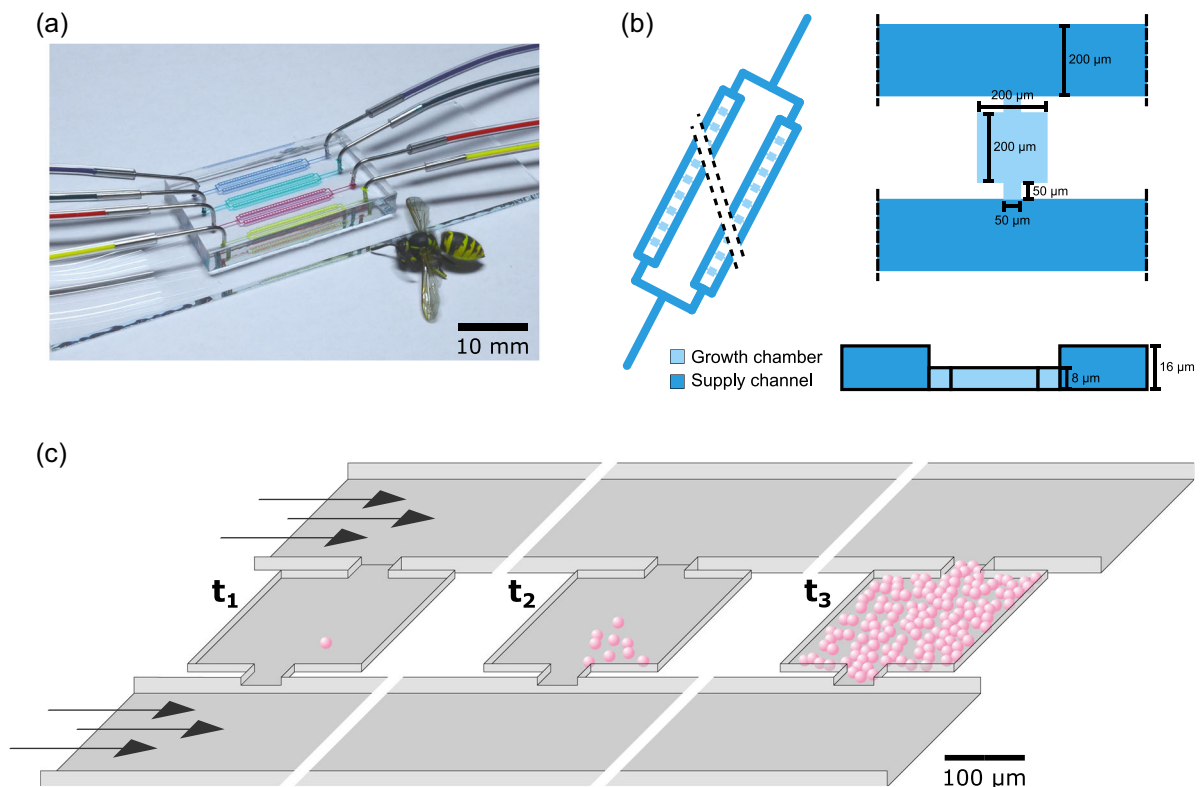


FIGURE 2 Design and working principle of MaSC. (a) Microfluidic PDMS-glass cultivation device for single-cell cultivation of mammalian suspension cell lines. To illustrate the device's dimensions a wasp is arranged next to the glass slide. (b) Schematic figure of the cultivation device: Each cultivation array consists of four parallel supply channels, between two of them 30 cultivation chambers with an area of $200 \times 200\ \mu\text{m}$ and a height of approximately $8\ \mu\text{m}$ are located. The adjacent supply channels are twice as high and show a width of $200\ \mu\text{m}$. (c) Three-dimensional illustration of the microfluidic device at different stages of the cultivation. t_1 , a single cell is seeded into the cultivation chamber; t_2 , the starter cell begins to proliferate and exponential growth starts; t_3 , approaching the end of a cultivation the chamber is filled with up to 170 cells [Color figure can be viewed at wileyonlinelibrary.com]

by-products are washed out through the outlet. This flow rate provides an exchange of the entire microfluidic device's volume about 10 times every minute, which assures constant environmental conditions over the whole cultivation course. Starting the cultivation with a small number of cells, the final cell number per cultivation chamber can reach up to 170 cells. Further exponential proliferation is only limited by the chamber's restricted volume of 3.2×10^{-7} ml.

3.2 | Device characteristics and functionality

CFD simulations were performed for detailed evaluation of fluid profiles inside the supply channels and cultivation chambers as well as the nutrient related cultivation conditions. With the presumed flow rate of $0.5 \mu\text{l}/\text{min}$ for each supply channel (4 channels per inlet),

a parabolic velocity profile and a maximal velocity of 30×10^{-4} m/s is observed inside the channels (Figure 3a). Due to the symmetric layout of the design as well as the narrow entrance, fluid flow inside the cultivation chamber is too slow to cause perturbations (Figure 3b). Thus, exchange of nutrients and by-products is predominantly diffusive. To examine whether cells inside a completely filled cultivation chamber can possibly experience limiting glucose concentration, another simulation was performed. With 171 cells per chamber and the specific glucose uptake rate of CHO-K1 cells, glucose concentration inside the chamber does not drop below 43.8 mmol/L in a steady-state (Figure 3c). Furthermore, a medium switch was simulated to determine the duration until full equilibrium from zero glucose to a cultivation sufficient glucose concentration of approximately 45 mmol/L is accomplished. The simulation indicates that after 25 s the cultivation chamber already shows half-maximal

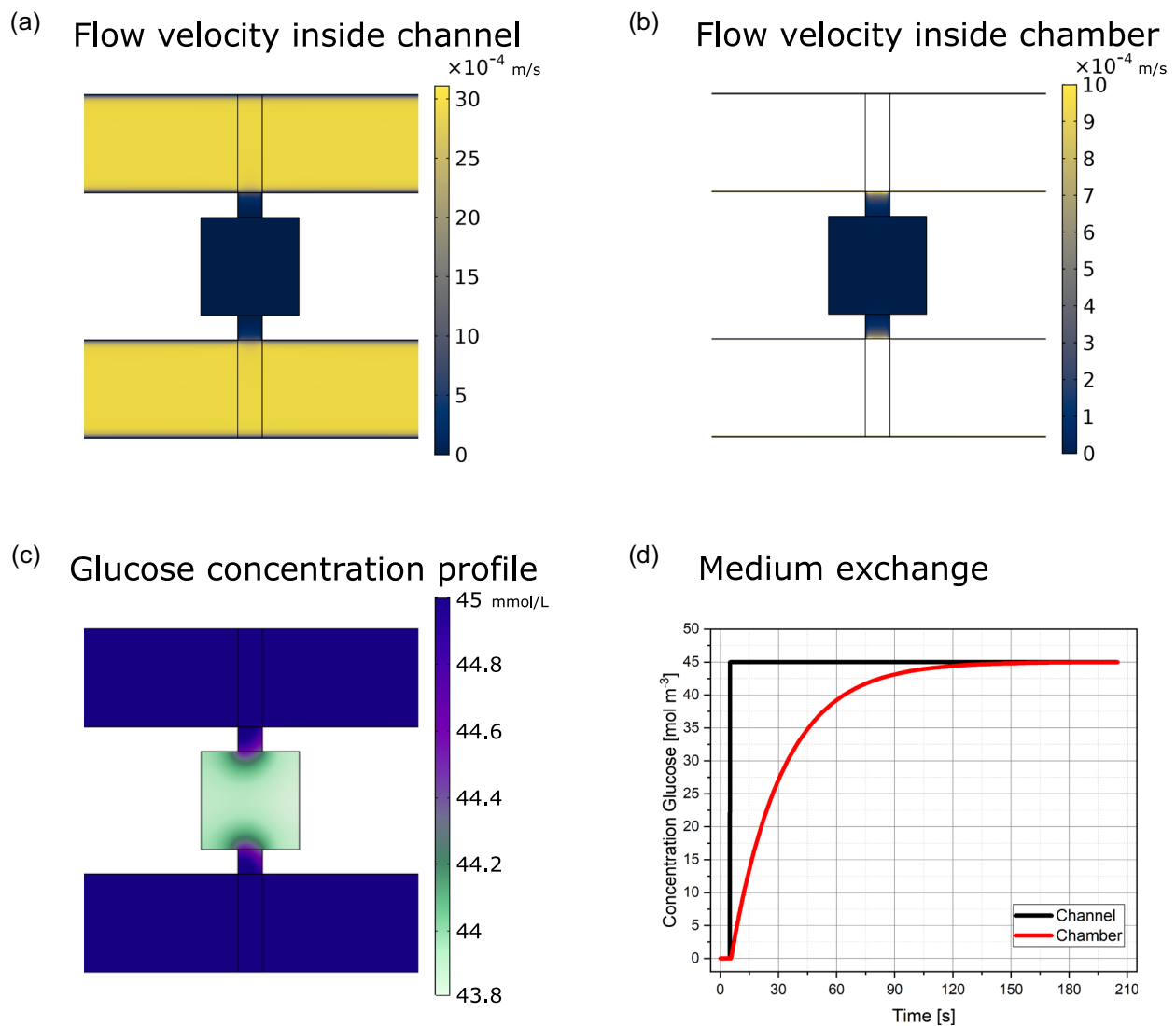


FIGURE 3 CFD simulations of flow and nutrient profile inside the microfluidic device. (a) Flow velocity inside supply channels. (b) Flow velocity inside representative cultivation chamber. (c) Glucose concentration profile assuming a steady-state at a cell number of 171 cells inside the chamber. (d) Glucose concentration inside the supply channels and cultivation chamber after quick medium change from non-glucose to 45 mmol/L glucose [Color figure can be viewed at wileyonlinelibrary.com]

glucose concentration, whereas 99.9% of the medium's glucose concentration is reached after approximately 150 s homogeneously throughout the whole chamber (Figure 3d).

3.3 | Mammalian single-cell cultivation

As CHO cell lines are the most frequently used cells in biopharmaceutical bioproduction processes (Walsh, 2018), CHO-K1 cells were used as a model system for the developed microfluidic device. For process near growth conditions, a commercially available cell culture medium, optimized for growth and production with CHO cell lines, was employed.

In three consecutive experiments, precultured cells were seeded into the microfluidic device. As cell loading is a mere statistical process, the number of loaded cultivation chambers varied in a range of 15–25 chambers. The number of cells in each chamber after loading varied between one and seven cells. As the medium exchange rate in the chambers is very high and to mimic the substrate and metabolite situation in standard bioreactors, a 1:1 mixture of fresh and conditioned medium was used as cultivation medium.

Cell growth in the chambers was analyzed on the colony level as well as on single-cell level. Here, colony growth rate μ_{colony} refers to the characteristic average values obtained from the cell number of each colony. In contrast, single-cell doubling times $t_{\text{D, single-cell}}$ refer to characteristic values obtained from single cells. In addition, single-cell area growth rates μ_{area} are obtained from single-cell area development. Under the assumption of an exponential growth behavior, each growth rate μ can be converted into the respective doubling time t_{D} and vice versa using Equation (1).

3.4 | Colony growth analysis

During the experiment, cells grew exponentially until the whole chamber was filled. The time-lapse sequence of Figure 4a illustrates an example of a growing microcolony. Random migration of cells inside the cultivation chambers could be observed (Video S1). After 6–7 days, a maximal cell number of approximately 150 cells per chamber is reached. At this state, cellular boundaries blur, as dividing cells are squeezed so tightly that individual cell membranes cannot be identified microscopically anymore. A cell number of 150 represents a cell density of 4.8×10^8 cells/ml inside the cultivation chamber, which is similar to the cellular density of human tissue (Skylar-Scott et al., 2019). In cultivation devices like flasks or bioreactors, cell culture does not reach these densities supposedly due to contact inhibition, microlimitations, and shear stress. In the microfluidic device, cells grow until they are tightly squeezed, thus it can be assumed that cells do not experience contact inhibition in the cultivation chamber, and therefore, contact inhibition may not be the cause for limited cell densities in other cultivation scales as well. Hence, we assume microlimitations and shear stress to be the critical factors restricting growth in flasks and bioreactors. Protuberances of

cellular membrane are observed during cultivation and are assumed to be caused by microvilli, extracellular matrix, endocytosis, and vesicle formation. Right before cell division, cells become sphere-shaped and smooth until cytokinesis takes place and the originated daughter cells start to show protuberances again (Figure 5a).

Depending on seeding cell density within the chambers, colony growth curves rise slightly shifted in the beginning, but initial cell number does not have a notable influence on growth progression of each microcolony (Figure 4b). Most likely, cell cycle distribution influences time until first cell division starts, as cells were randomly distributed across cell cycle phases before loading the microfluidic device. This can result in a delay of up to 20 h for cells being in G1 phase compared to cells in G2 phase, which start mitosis very rapidly. A lag-phase for chambers with low initial cell number seems unlikely, given that semi-logarithmic growth curves show exponential growth right from the experimental start (Figure S1). Linear fits show similar colony growth rates between 0.75 and 0.95 day⁻¹ for the colonies presented here (Table S1).

3.5 | Single-cell growth analysis

Besides evaluating microcolony growth, MaSC explicitly enables single-cell data acquisition (Figure 5a). Therefore, we determined single-cell doubling times and single-cell area development to analyze cellular division behavior throughout the microcolony. As can be seen in Figure 5b, the distribution of single-cell doubling times $t_{\text{D, single-cell}}$ underlies certain variabilities, especially the distribution width differs and rare cellular events can be identified; most of them show an extended doubling time longer than 25 h, only few fall below 10 h. Looking at the respective mean doubling time, they alternate between 14.3 and 19.6 h, whereas the cumulative determined mean doubling time is 15.9 h (Figure S2). Looking at colony A.5, B.1, and B.3 (Figure 5b) shows that starting cell number influences t_{D} only marginally as each colony started with a cell number ≥ 5 and broadness as well as mean $t_{\text{D, single-cell}}$ differ clearly. As the correlation coefficient for starting cell number and mean t_{D} is $R = 0.394$, only a weak trend can be assumed (Figure S3).

Figure 5c shows the single-cell area development of two cells originated from a mutual progenitor cell. The area increase shows small variations, the corresponding μ_{area} differ between 1.14 and 1.39 day⁻¹. Noteworthy, second-generation cells originated from the slower initial cell both show slightly lower area growth rates than those that originated from the faster initial cell. Comparing the area growth rate with the corresponding doubling times of the analyzed cells shows no correlation between μ_{area} and $t_{\text{D, single-cell}}$ (Figure S4). One explanation might be the continuous secretion of vesicles, which makes the cellular area a continuously fluctuating property and thus the exact determination of the cell area difficult. Another more relevant reason lies in the dependency of cellular growth on cell cycle phases combined with the cell's mechanism to ensure constant cellular size over generations. In general, there are three different models that describe how cells can reach size homeostasis.

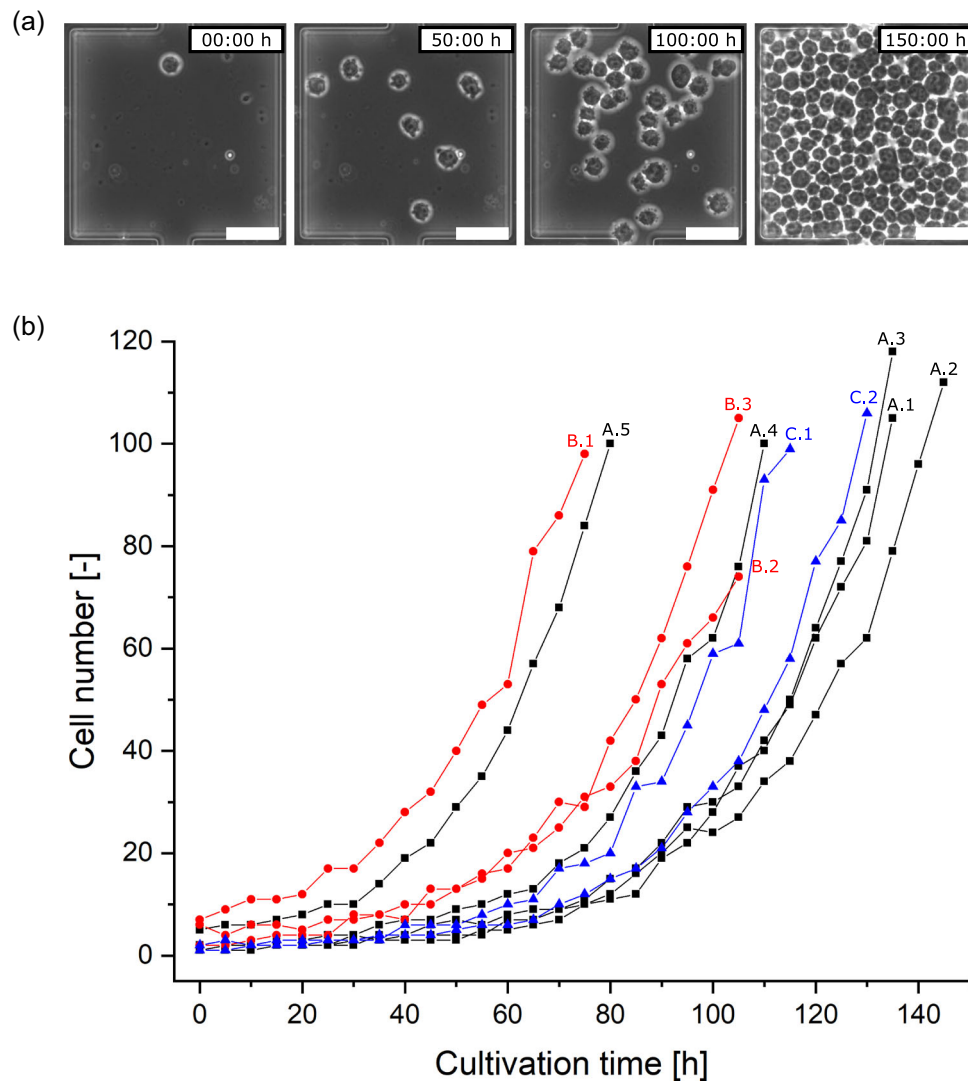


FIGURE 4 Colony growth of CHO-K1 cells at constant environmental conditions. (a) Time-lapse image sequence showing microfluidic growth of one initial CHO-K1 cell to a microcolony over an experimental duration of 150 h (scale bar = 50 μm). (b) Colony growth of CHO-K1 microcolonies. Here, 10 selected chambers from three technical replicates are shown. Black squares (A.1–A.5), red dots (B.1–B.3), and blue triangles (C.1–C.2) represent one technical replicate each. Depending on starting cell number and cell cycle distribution, exponential growth starts slightly shifted between the microcolonies [Color figure can be viewed at wileyonlinelibrary.com]

The sizer-mechanism controls the beginning of mitosis by a size threshold, for the adder-mechanism, the cell size increases by a constant amount independent of initial cell size, and with the timer-mechanism cells grow exponentially for a constant duration (Cadart et al., 2018; Vuaridel-Thurre et al., 2020). To determine if this correlation applies to the area development of CHO-K1 cells, we compared the cell area of single cells at their birth and at their mitosis. For better clearness, the data in Figure 5d were normalized by the average cell area at mitosis. As sizer-cells undergo mitosis at a consistent cell size independently from their size immediately after mitosis, this mechanism can be illustrated by a horizontal line. The dashed line with a slope of 1 and an intercept of 0.5 in Figure 5d represents cells with adder-behavior while timer-cells are consistent with the dashed line through the origin and a slope of 2 (assuming exponential cell growth). Comparing the single-cell data with the

expected trends, an adder-mechanism to assure size homeostasis can be identified for the here analyzed CHO-K1 cells. In addition, a correlation between cell $\text{area}_{\text{birth}}$ and the ratio of cell $\text{area}_{\text{mitosis}}$ and cell $\text{area}_{\text{birth}}$ casts a timer mechanism in doubt (Figure S5). This behavior is in accordance with already analyzed mammalian cells, which were analyzed in an microfluidic flow-through system (Cadart et al., 2018).

Growth rates obtained from single-cell level are noteworthy higher than those obtained from colony level (Table S1). Here, the main reason for this discrepancy is the technical insufficiencies of the developed microfluidic setup, as occasionally single cells can escape the cultivation chamber by random movement reducing the apparent colony growth rate. Such events can be identified as bends in some colonies' growth curves (Figure 4b). Therefore, the here determined colony growth rates underestimate growth rates which would be

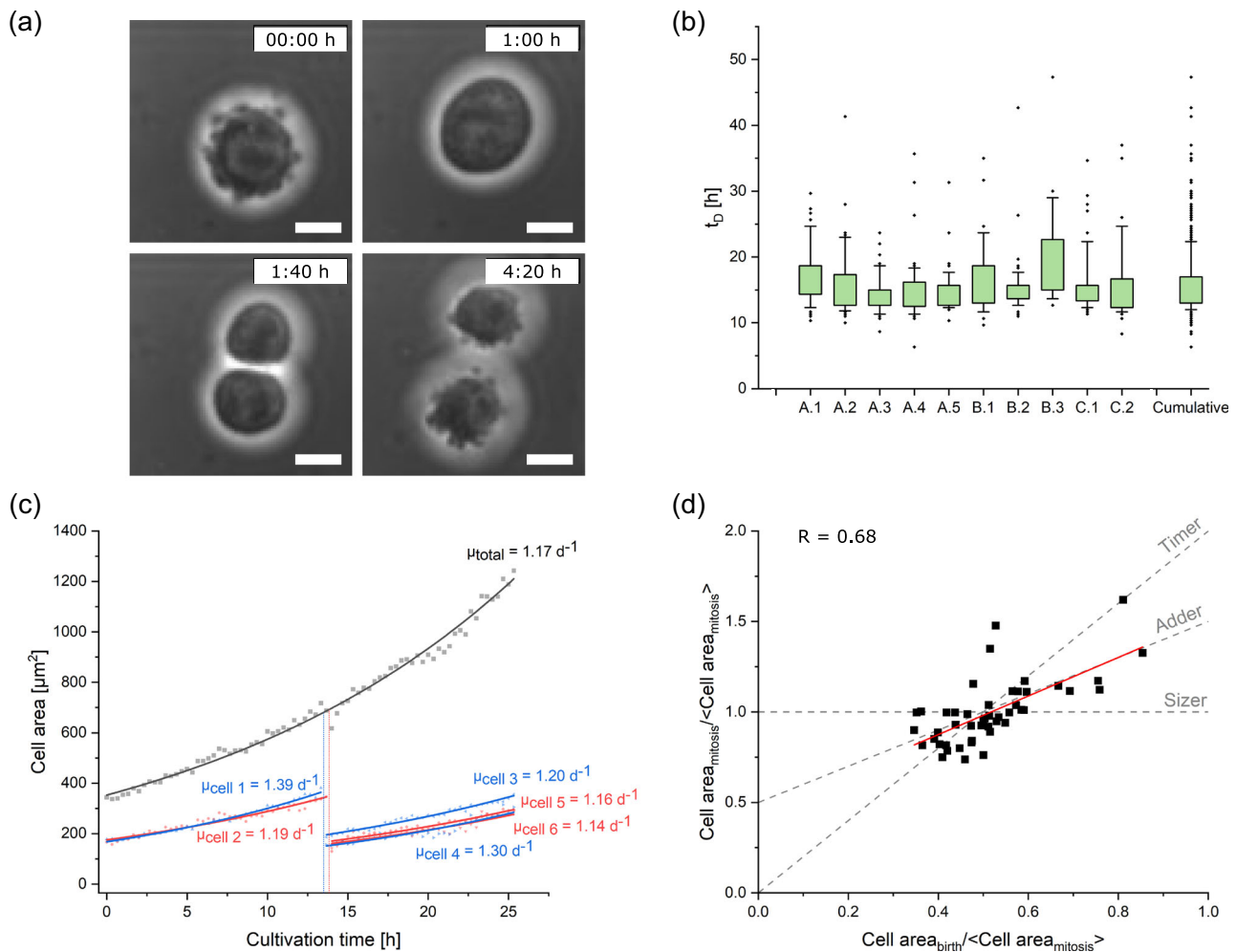


FIGURE 5 (a) Cell division event for illustration of the accompanying cellular morphological changes (scale bar = 10 μm). (b) Distribution of single-cell doubling times of the microcolonies depicted in Figure 4 complemented with a cumulative t_D distribution over all doubling events. The colored segment marks the interquartile range from 25% to 75%. The whiskers represent the 10% and 90% percentile and the tilted squares mark rare cellular events. (c) Determination of area growth rates of single cells from colony A.5. The analysis started with the origin of Cell 1 and Cell 2 from one mutual progenitor cell and was conducted for 25 h in intervals of 20 min. Depicted are the colony's total cell area and the individual cells' areas. By exponential fit specific growth rates were determined from increasing cell area. (d) Cell size homeostasis analysis of single cells from colony A.1. To determine which of the conventional cell size homeostasis models (timer, adder, and sizer) applies to CHO-K1 cells, the correlation between cell area at birth and cell area at mitosis was analyzed. For clearness, all area data were normalized by the average cell area at mitosis. The trend lines (dashed gray) show the expected trends in case of timer, adder, and sizer behavior [Color figure can be viewed at wileyonlinelibrary.com]

obtained without the described cell loss. Nevertheless, they match growth rates derived from classic shake flask or lab-scale bioreactor cultivations of CHO-K1 suspension cells (data not shown).

Consistencies between microfluidic cultivation and larger cultivation scales have already been described before by Kolnik et al. (2012), who compared the growth of adherent CHO cells in a microfluidic device with six-well plate cultivation. Transferring common cultivation scales into microfluidic devices does not always show comparable growth behavior, as steady perfusion leads to constant washout of secreted molecules and beneficial factors (Taheri-Araghi et al., 2015). Preliminary tests showed that CHO-K1 cells do not grow in fresh medium (data not shown). For this reason, we supplemented the commercial medium with an already conditioned one in our study.

Other examples like the cultivation of microbial production hosts such as *Corynebacterium glutamicum* showed significantly higher growth rates in microfluidic single-cell cultivation compared to lab-scale cultivations (Fritzsche et al., 2013; Grünberger et al., 2013), which most likely result from the growth-promoting environmental conditions concerning nutrient supply inside the applied microfluidic devices.

3.6 | Cell-to-cell heterogeneity and rare cellular events

During CHO-K1 single-cell cultivation described above, various examples of heterogeneous behavior between isogenic cells have been

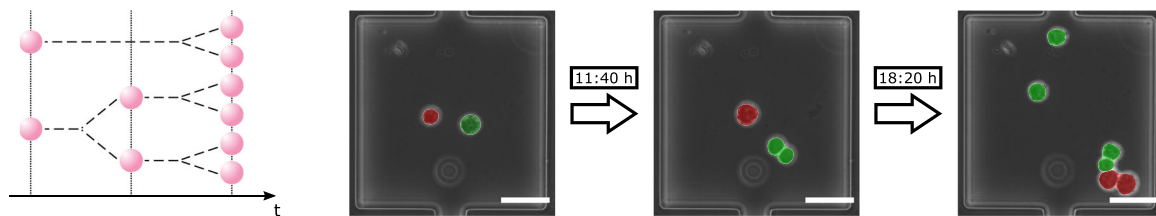
observed. Considering the rare cellular events of Figure 5b, variations in cell division happen in every cultivation but only single-cell analysis makes them visible. In the following, some of these outliers with $t_D > 25$ h were analyzed more closely on a single-cell level.

Originating from a common mother cell, the subsequent doubling time of the daughter cells (first-generation) varied strongly (Figure 6a and Video S2). Although one daughter cell (depicted in red) grew in cell volume for another 18 h until it finally underwent cell division, the other daughter cell (depicted in green) and its progenies (second-generation) finished two rounds of cell division.

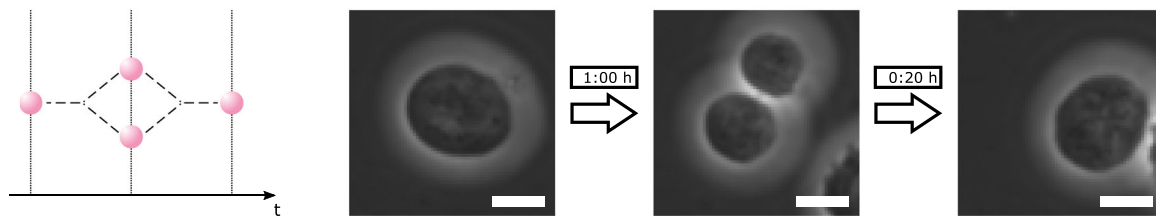
Delay in proliferation of single cells is not the only incident being observed. Cell division can also be aborted or even reversed in the

final step of cytokinesis. After a performed division, one daughter cell reabsorbed the other (Figure 6b and Video S3). This observation in some respects contradicts the hypothesis of the point of no return in the eukaryotic cell cycle. One explanation might be the occurrence of errors during mitosis so that reabsorption acts like a safety mechanism against formation of defective progenies (Potapova et al., 2006). Few cells did not even start cytokinesis but nevertheless underwent DNA replication. Hence, huge polynuclear cells appear (Figure 6c and Video S4). As they also occur in microcolonies where other cells show perfectly normal proliferation, detrimental environmental conditions are highly unlikely as a cause for polynucleation. Surprisingly, in some cases, these polynuclear cells

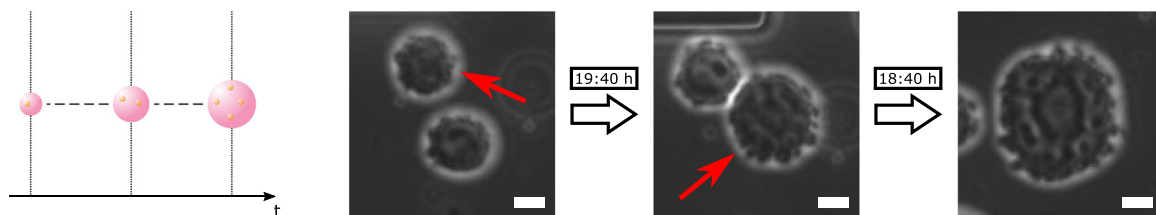
(a) Unequal division time



(b) Reabsorption



(c) Polynucleation



(d) Quadruple division

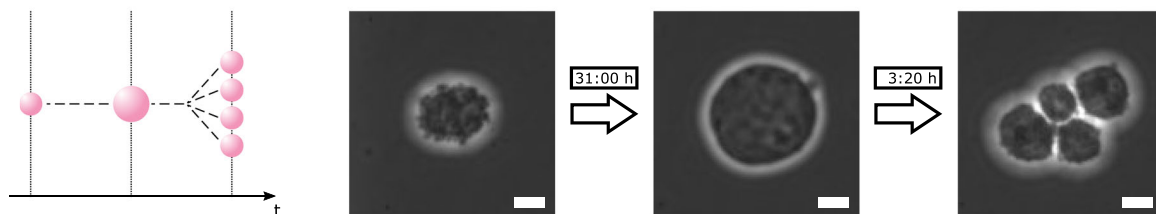


FIGURE 6 Examples of cell-to-cell heterogeneity and rare cellular events during mammalian single-cell cultivation. (a) Genetically identical cells differ in their doubling time by 18 h (scale bar = 50 μ m). (b) One cell reabsorbs the second cell immediately after cell division (scale bar = 10 μ m). (c) Absence of cell division leads to immense polynuclear cells (red arrow; scale bar = 10 μ m). (d) One cell divides into four daughter cells which all are viable (scale bar = 10 μ m) [Color figure can be viewed at wileyonlinelibrary.com]

eventually pass through cytokinesis. Sometimes, these cells divide into two daughter cells which randomly are polynuclear as well. In other cases, polynuclear cells divide into multiple mononuclear cells (Figure 6d and Video S5).

We assume that the—partly surprising—incidences being described in Figure 6 are not caused by the microfluidic cultivation condition, but generally occur in CHO cell culture including bioreactors and biopharmaceutical processes, and contribute to population heterogeneity.

3.7 | Future applications

The introduction of MaSC showed that long-term cultivation of mammalian suspension cells in chamber-based microfluidic devices is feasible. Besides growth analysis on colony level, also single-cell behavior can be examined and heterogeneity among individual cells can be revealed. Prospectively, MaSC may not only be applied for growth studies but also for systematic investigation of population heterogeneity, cellular transfection, or cell-to-cell interactions in basic research (Figure 7a). In a more application-orientated way, our tool can be installed in different disciplines of (bio)pharmaceutical research (Figure 7b), ranging from the first screening of potential drug components and the development of new cell lines for industrial production to stem cell research. Particularly for the expansion of monoclonal cell lines descending from a single cell with beneficial growth or production properties, microfluidic approaches are highly promising but difficult to realize. In this context integration of optical tweezers for single-cell isolation is a promising approach, but has mainly been employed for bacterial applications in microfluidic cultivation chambers so far (Luro et al., 2020; Probst et al., 2013). With reference to bioproduction processes,

systematic design-of-experiment-based media development and process optimization represent possible fields of application for MaSC (Figure 7c). Eventually, single-cell cultivation of mammalian cells can even serve as a starting point for bioprocess development in terms of scale-down approaches. However, beforehand comparability of microfluidic cultivation to shake flasks and lab-scale bioreactors needs to be shown by in-depth validation studies to ensure transferability from the single-cell level.

Before systematic application, there are still technical aspects to improve and obstacles to overcome. First, better cell retention needs to be achieved by adapting the device's design to prevent cell loss from the cultivation chamber due to the movement of the cells. Here, narrowing the chambers' entrances or placing physical barriers in front of the entrances might be a promising approach. Likewise, cell loading efficiency must be increased. Concerning experimental data evaluation, automated image analysis appears worthwhile, as cell number, doubling times, and cell area were determined manually and therefore are error-prone and time-consuming.

4 | CONCLUSION

The MaSC platform presented in this study allows long-term cultivation of mammalian suspension cells starting from a single cell and makes microfluidic systems available for industrially relevant biopharmaceutical applications. Microfluidic cultivation ensures controlled environmental conditions while live-cell imaging enables spatiotemporal resolution of cellular behavior. Consequently, not only population dynamics but also individual single-cell events can be investigated. The device's modular concept permits scalability from currently 60 individual cultivation chambers up to several hundred to increase the amount of statistical data per run. Alongside its other

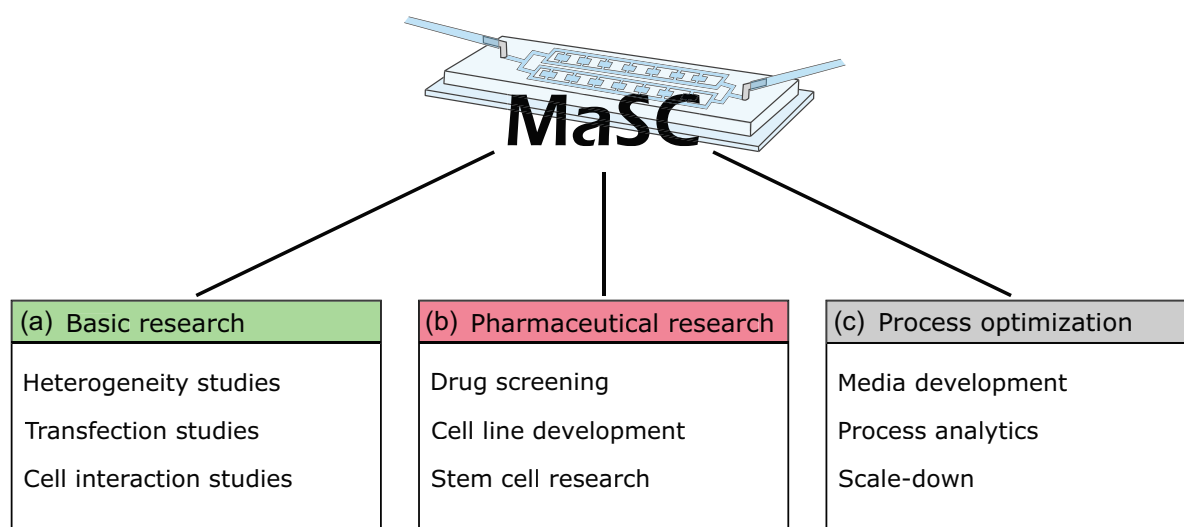


FIGURE 7 Examples of application fields for MaSC. (a) In basic research, MaSC can be applied for heterogeneity studies, investigating transfection, and analyzing cellular interactions. (b) In pharmaceutical research especially drug screening, cell line development, and stem cell research approaches can be realized with MaSC technology. (c) In bioprocess research, MaSC can simplify media development, function as process analytical tool, or prospectively be the starting point for scale-down approaches [Color figure can be viewed at [wileyonlinelibrary.com](https://onlinelibrary.wiley.com)]

benefits, this aspect makes MaSC suitable for analytical studies of industrially relevant cell lines.

The focus of our study was establishing microfluidic single-cell cultivation for suspension cell lines. Growth analysis was performed on the microcolony as well as on a single-cell level and showed reproducible growth rates. Several, partly very surprising, incidences resulting in population heterogeneity have been observed on a single-cell level and were investigated subsequently. This lays the foundation for systematic single-cell studies for suspension cell lines in the fields of basic research, cell line development and characterization, stability studies, and bioprocess development.

For the future, it is interesting to extend the MaSC platform by adding tools that allow epigenetic and functional genomic analysis of individual cells and to include analysis of product quality when using recombinant production cell lines. This will enable an increased understanding of the full scope and consequences of the observed cellular heterogeneities and open the door for the development of stable (production) cell lines and homogeneous bioprocesses (Schmitz et al., 2019).

ACKNOWLEDGMENTS

Parts of this study were performed at the cleanroom facilities of the Department of Biophysics and Nanoscience as well as the Department for Physics of Supramolecular Systems and Surfaces at Bielefeld University. Cell culture maintenance was performed with help of the members of the Cell Culture Technology group at Bielefeld University. Preliminary single-cell cultivation experiments have been performed by Sebastian Perez Knoche and Lars Niklas Halle. The authors would like to thank all for help and support. Open access funding enabled and organized by Projekt DEAL.

AUTHOR CONTRIBUTIONS

Conception and design: Julian Schmitz, Sarah Täuber, and Alexander Grünberger. *Acquisition of data:* Julian Schmitz and Christoph Westerwalbesloh. *Analysis and interpretation of data:* Julian Schmitz, Christoph Westerwalbesloh, Thomas Noll, and Alexander Grünberger. *Writing:* Julian Schmitz, Christoph Westerwalbesloh, and Alexander Grünberger. *Final proof reading:* Julian Schmitz, Sarah Täuber, Christoph Westerwalbesloh, Eric von Lieres, Thomas Noll, and Alexander Grünberger. *Providing resources:* Eric von Lieres, Thomas Noll, and Alexander Grünberger.

DATA AVAILABILITY STATEMENT

The data that support the findings of this study are available from the corresponding author upon reasonable request.

ORCID

Julian Schmitz  <https://orcid.org/0000-0001-9243-150X>

Christoph Westerwalbesloh  <https://orcid.org/0000-0002-3064-7425>

Eric von Lieres  <https://orcid.org/0000-0002-0309-8408>

Thomas Noll  <http://orcid.org/0000-0003-0748-3423>

Alexander Grünberger  <http://orcid.org/0000-0002-7564-4957>

REFERENCES

- Binder, D., Probst, C., Grünberger, A., Hilgers, F., Loeschcke, A., Jaeger, K.-E., Kohlheyer, D., & Drepper, T. (2016). Comparative single-cell analysis of different *E. coli* expression systems during microfluidic cultivation. *PLoS One*, 11(8), e0160711. <https://doi.org/10.1371/journal.pone.0160711>
- Bjork, S. M., Sjöstrom, S. L., Andersson-Svahn, H., & Joensson, H. N. (2015). Metabolite profiling of microfluidic cell culture conditions for droplet based screening. *Biomechanics*, 9(4), 044128. <https://doi.org/10.1063/1.4929520>
- Burmeister, A., Hilgers, F., Langner, A., Westerwalbesloh, C., Kerkhoff, Y., Tenhaef, N., Drepper, T., Kohlheyer, D., von Lieres, E., Noack, S., & Grünberger, A. (2018). A microfluidic co-cultivation platform to investigate microbial interactions at defined microenvironments. *Lab on a Chip*, 19(1), 98–110. <https://doi.org/10.1039/c8lc00977e>
- Cadart, C., Monnier, S., Grilli, J., Sáez, P. J., Srivastava, N., Attia, R., Terriac, E., Baum, B., Cosentino-Lagomarsino, M., & Piel, M. (2018). Size control in mammalian cells involves modulation of both growth rate and cell cycle duration. *Nature Communications*, 9(1), 3275. <https://doi.org/10.1038/s41467-018-05393-0>
- Comesaña, J. F., Otero, J. J., García, E., & Correa, A. (2003). Densities and viscosities of ternary systems of water + glucose + sodium chloride at several temperatures. *Journal of Chemical & Engineering Data*, 48(2), 362–366. <https://doi.org/10.1021/je020153x>
- Delvigne, F., & Goffin, P. (2014). Microbial heterogeneity affects bioprocess robustness: Dynamic single-cell analysis contributes to understanding of microbial populations. *Biotechnology Journal*, 9(1), 61–72. <https://doi.org/10.1002/biot.201300119>
- Dettinger, P., Frank, T., Etzrodt, M., Ahmed, N., Reimann, A., Trenzinger, C., Loeffler, D., Kokkaliaris, K. D., Schroeder, T., & Tay, S. (2018). Automated microfluidic system for dynamic stimulation and tracking of single cells. *Analytical Chemistry*, 90(18), 10695–10700. <https://doi.org/10.1021/acs.analchem.8b00312>
- Di Carlo, D., Wu, L. Y., & Lee, L. P. (2006). Dynamic single cell culture array. *Lab on a Chip*, 6(11), 1445–1449. <https://doi.org/10.1039/b605937f>
- Du, G., Fang, Q., & den Toonder, J. M. J. (2016). Microfluidics for cell-based high throughput screening platforms—A review. *Analytica Chimica Acta*, 903, 36–50. <https://doi.org/10.1016/j.aca.2015.11.023>
- Fritzsche, F. S. O., Rosenthal, K., Kampert, A., Howitz, S., Dusny, C., Blank, L. M., & Schmid, A. (2013). Picoliter nDEP traps enable time-resolved contactless single bacterial cell analysis in controlled microenvironments. *Lab on a Chip*, 13(3), 397–408. <https://doi.org/10.1039/c2lc41092c>
- Frye, C., Deshpande, R., Estes, S., Francissen, K., Joly, J., Lubiniecki, A., Munro, T., Russell, R., Wang, T., & Anderson, K. (2016). Industry view on the relative importance of “clonality” of biopharmaceutical-producing cell lines. *Biologicals*, 44(2), 117–122. <https://doi.org/10.1016/j.biologics.2016.01.001>
- Gao, Y., Li, P., & Pappas, D. (2013). A microfluidic localized, multiple cell culture array using vacuum actuated cell seeding: Integrated anticancer drug testing. *Biomedical Microdevices*, 15(6), 907–915. <https://doi.org/10.1007/s10544-013-9779-3>
- Grilo, A. L., & Mantalaris, A. (2019). Apoptosis: A mammalian cell bioprocessing perspective. *Biotechnology Advances*, 37(3), 459–475. <https://doi.org/10.1016/j.biotechadv.2019.02.012>
- Grünberger, A., van Ooyen, J., Paczia, N., Rohe, P., Schiendzielorz, G., Eggeling, L., Wiechert, W., Kohlheyer, D., & Noack, S. (2013). Beyond growth rate 0.6: *Corynebacterium glutamicum* cultivated in highly diluted environments. *Biotechnology and Bioengineering*, 110(1), 220–228. <https://doi.org/10.1002/bit.24616>
- Grünberger, A., Probst, C., Helfrich, S., Nanda, A., Stute, B., Wiechert, W., Lieres, E. von, Nöh, K., Frunzke, J., & Kohlheyer, D. (2015). Spatiotemporal microbial single-cell analysis using a high-throughput

- microfluidics cultivation platform. *Cytometry Part A*, 87(12), 1101–1115. <https://doi.org/10.1002/cyto.a.22779>
- Grünberger, A., Probst, C., Heyer, A., Wiechert, W., Frunzke, J., & Kohlheyer, D. (2013). Microfluidic picoliter bioreactor for microbial single-cell analysis: Fabrication, system setup, and operation. *Journal of Visualized Experiments*, (82):e50560. <https://doi.org/10.3791/50560>
- Grünberger, A., Wiechert, W., & Kohlheyer, D. (2014). Single-cell microfluidics: Opportunity for bioprocess development. *Current Opinion in Biotechnology*, 29, 15–23. <https://doi.org/10.1016/j.copbio.2014.02.008>
- Halldorsson, S., Lucumi, E., Gómez-Sjöberg, R., & Fleming, R. M. T. (2015). Advantages and challenges of microfluidic cell culture in polydimethylsiloxane devices. *Biosensors & Bioelectronics*, 63, 218–231. <https://doi.org/10.1016/j.bios.2014.07.029>
- Karakas, H. E., Kim, J., Park, J., Oh, J. M., Choi, Y., Gozuacik, D., & Cho, Y.-K. (2017). A microfluidic chip for screening individual cancer cells via eavesdropping on autophagy-inducing crosstalk in the stroma niche. *Scientific Reports*, 7(1), 2050. <https://doi.org/10.1038/s41598-017-02172-7>
- Kolnik, M., Tsimring, L. S., & Hasty, J. (2012). Vacuum-assisted cell loading enables shear-free mammalian microfluidic culture. *Lab on a Chip*, 12(22), 4732–4737. <https://doi.org/10.1039/c2lc40569e>
- Le, H., Kabbur, S., Pollastrini, L., Sun, Z., Mills, K., Johnson, K., Karypis, G., & Hu, W.-S. (2012). Multivariate analysis of cell culture bioprocess data—Lactate consumption as process indicator. *Journal of Biotechnology*, 162(2–3), 210–223. <https://doi.org/10.1016/j.jbiotec.2012.08.021>
- Lecault, V., White, A. K., Singhal, A., & Hansen, C. L. (2012). Microfluidic single cell analysis: From promise to practice. *Current Opinion in Chemical Biology*, 16(3–4), 381–390. <https://doi.org/10.1016/j.cbpa.2012.03.022>
- Li, R., Lv, X., Zhang, X., Saeed, O., & Deng, Y. (2016). Microfluidics for cell–cell interactions: A review. *Frontiers of Chemical Science and Engineering*, 10(1), 90–98. <https://doi.org/10.1007/s11705-015-1550-2>
- Lin, C.-H., Hsiao, Y.-H., Chang, H.-C., Yeh, C.-F., He, C.-K., Salm, E. M., Chen, C., Chiu, I.-M., & Hsu, C.-H. (2015). A microfluidic dual-well device for high-throughput single-cell capture and culture. *Lab on a Chip*, 15(14), 2928–2938. <https://doi.org/10.1039/c5lc00541h>
- Lindström, S., & Andersson-Svahn, H. (2010). Overview of single-cell analyses: Microdevices and applications. *Lab on a Chip*, 10(24), 3363–3372. <https://doi.org/10.1039/c0lc00150c>
- Luni, C., Giullitti, S., Serena, E., Ferrari, L., Zambon, A., Gagliano, O., Giobbe, G. G., Michielin, F., Knöbel, S., Bosio, A., & Elvassore, N. (2016). High-efficiency cellular reprogramming with microfluidics. *Nature Methods*, 13(5), 446–452. <https://doi.org/10.1038/nmeth.3832>
- Luro, S., Potvin-Trottier, L., Okumus, B., & Paulsson, J. (2020). Isolating live cells after high-throughput, long-term, time-lapse microscopy. *Nature Methods*, 17(1), 93–100. <https://doi.org/10.1038/s41592-019-0620-7>
- Marques, M. P., & Szita, N. (2017). Bioprocess microfluidics: Applying microfluidic devices for bioprocessing. *Current Opinion in Chemical Engineering*, 18, 61–68. <https://doi.org/10.1016/j.coche.2017.09.004>
- Mehling, M., & Tay, S. (2014). Microfluidic cell culture. *Current Opinion in Biotechnology*, 25, 95–102. <https://doi.org/10.1016/j.copbio.2013.10.005>
- Nolan, R. P., & Lee, K. (2011). Dynamic model of CHO cell metabolism. *Metabolic Engineering*, 13(1), 108–124. <https://doi.org/10.1016/j.ymben.2010.09.003>
- Phoenix, D. (1997). *Introductory mathematics for the life sciences*. CRC Press.
- Postiglione, L., Santorelli, M., Tumaini, B., & di Bernardo, D. (2016). From a discrete to continuous actuation for improved real-time control of gene expression in mammalian cells. *IFAC-PapersOnLine*, 49(26), 14–19. <https://doi.org/10.1016/j.ifacol.2016.12.096>
- Potapova, T. A., Daum, J. R., Pittman, B. D., Hudson, J. R., Jones, T. N., Satinover, D. L., Stukenberg, P. T., & Gorbsky, G. J. (2006). The reversibility of mitotic exit in vertebrate cells. *Nature*, 440(7086), 954–958. <https://doi.org/10.1038/nature04652>
- Probst, C., Grünberger, A., Wiechert, W., & Kohlheyer, D. (2013). Microfluidic growth chambers with optical tweezers for full spatial single-cell control and analysis of evolving microbes. *Journal of Microbiological Methods*, 95(3), 470–476. <https://doi.org/10.1016/j.mimet.2013.09.002>
- Raimes, W., Rubi, M., Super, A., Marques, M. P. C., Veraitch, F., & Szita, N. (2017). Transfection in perfused microfluidic cell culture devices: A case study. *Process Biochemistry*, 59(Pt B), 297–302. <https://doi.org/10.1016/j.procbio.2016.09.006>
- Rowat, A. C., Bird, J. C., Agresti, J. J., Rando, O. J., & Weitz, D. A. (2009). Tracking lineages of single cells in lines using a microfluidic device. *Proceedings of the National Academy of Sciences of the United States of America*, 106(43), 18149–18154. <https://doi.org/10.1073/pnas.0903163106>
- Schindelin, J., Arganda-Carreras, I., Frise, E., Kaynig, V., Longair, M., Pietzsch, T., Preibisch, S., Rueden, C., Saalfeld, S., Schmid, B., Tinevez, J.-Y., White, D. J., Hartenstein, V., Eliceiri, K., Tomancak, P., & Cardona, A. (2012). Fiji: An open-source platform for biological-image analysis. *Nature Methods*, 9(7), 676–682. <https://doi.org/10.1038/nmeth.2019>
- Schmitz, J., Noll, T., & Grünberger, A. (2019). Heterogeneity studies of mammalian cells for bioproduction: From tools to application. *Trends in Biotechnology*, 37(6), 645–660. <https://doi.org/10.1016/j.tibtech.2018.11.007>
- Skyilar-Scott, M. A., Uzel, S. G. M., Nam, L. L., Ahrens, J. H., Truby, R. L., Damaraju, S., & Lewis, J. A. (2019). Biomanufacturing of organ-specific tissues with high cellular density and embedded vascular channels. *Science Advances*, 5(9), eaaw2459. <https://doi.org/10.1126/sciadv.aaw2459>
- Taheri-Araghi, S., Brown, S. D., Sauls, J. T., McIntosh, D. B., & Jun, S. (2015). Single-cell physiology. *Annual Review of Biophysics*, 44, 123–142. <https://doi.org/10.1146/annurev-biophys-060414-034236>
- Täuber, S., von Lieres, E., & Grünberger, A. (2020). Dynamic environmental control in microfluidic single-cell cultivations: From concepts to applications. *Small*, 16, e1906670. <https://doi.org/10.1002/sml.201906670>
- Templer, R. H., & Ces, O. (2008). New frontiers in single-cell analysis. *Journal of the Royal Society Interface*, 5(Suppl 2), S111–S112. <https://doi.org/10.1098/rsif.2008.0279.focus>
- Unthan, S., Grünberger, A., van Ooyen, J., Gätgens, J., Heinrich, J., Paczia, N., Wiechert, W., Kohlheyer, D., & Noack, S. (2014). Beyond growth rate 0.6: What drives *Corynebacterium glutamicum* to higher growth rates in defined medium. *Biotechnology and Bioengineering*, 111(2), 359–371. <https://doi.org/10.1002/bit.25103>
- Vuaridel-Thurre, G., Vuaridel, A. R., Dhar, N., & McKinney, J. D. (2020). Computational analysis of the mutual constraints between single-cell growth and division control models. *Advanced Biosystems*, 4(2), e1900103. <https://doi.org/10.1002/adbi.201900103>
- Walsh, G. (2018). Biopharmaceutical benchmarks 2018. *Nature Biotechnology*, 36(12), 1136–1145. <https://doi.org/10.1038/nbt.4305>
- Wang, D., & Bodovitz, S. (2010). Single cell analysis: The new frontier in 'omics'. *Trends in Biotechnology*, 28(6), 281–290. <https://doi.org/10.1016/j.tibtech.2010.03.002>
- Westerwalbesloh, C., Grünberger, A., Stute, B., Weber, S., Wiechert, W., Kohlheyer, D., & von Lieres, E. (2015). Modeling and CFD simulation of nutrient distribution in picoliter bioreactors for bacterial growth studies on single-cell level. *Lab on a Chip*, 15(21), 4177–4186. <https://doi.org/10.1039/c5lc00646e>
- Westerwalbesloh, C., Grünberger, A., Wiechert, W., Kohlheyer, D., & von Lieres, E. (2017). Coarse-graining bacteria colonies for modelling critical solute distributions in picolitre bioreactors for

- bacterial studies on single-cell level. *Microbial Biotechnology*, 10(4), 845–857. <https://doi.org/10.1111/1751-7915.12708>
- Wheeler, A. R., Thronset, W. R., Whelan, R. J., Leach, A. M., Zare, R. N., Liao, Y. H., Farrell, K., Manger, I. D., & Daridon, A. (2003). Microfluidic device for single-cell analysis. *Analytical Chemistry*, 75(14), 3581–3586. <https://doi.org/10.1021/ac0340758>
- Woodruff, K., & Maerkl, S. J. (2016). A high-throughput microfluidic platform for mammalian cell transfection and culturing. *Scientific Reports*, 6, 23937. <https://doi.org/10.1038/srep23937>
- Wurm, F. M. (2004). Production of recombinant protein therapeutics in cultivated mammalian cells. *Nature Biotechnology*, 22(11), 1393–1398. <https://doi.org/10.1038/nbt1026>
- Wurm, F. (2013). CHO quasispecies—Implications for manufacturing processes. *Processes*, 1(3), 296–311. <https://doi.org/10.3390/pr1030296>
- Yin, H., & Marshall, D. (2012). Microfluidics for single cell analysis. *Current Opinion in Biotechnology*, 23(1), 110–119. <https://doi.org/10.1016/j.copbio.2011.11.002>

SUPPORTING INFORMATION

Additional Supporting Information may be found online in the supporting information tab for this article.

How to cite this article: Schmitz J, Täuber S, Westerwalbesloh C, von Lieres E, Noll T, Grünberger A. Development and application of a cultivation platform for mammalian suspension cell lines with single-cell resolution. *Biotechnology and Bioengineering*. 2020;1–14. <https://doi.org/10.1002/bit.27627>